All-optical beam control with high speed using image-induced blazed gratings in coherent media

L. Zhao,[1,*] Wenhui Duan,[1] and S. F. Yelin[2,3]
[1]*Department of Physics, Tsinghua University, Beijing 100084, People's Republic of China*
[2]*Department of Physics, University of Connecticut, Storrs, Connecticut 06269, USA*
[3]*ITAMP, Harvard-Smithsonian Center for Astrophysics, Cambridge, Massachusetts 02138, USA*
(Received 5 April 2010; published 12 July 2010)

Based on the theory of electromagnetically induced transparency, we study the formation of all-optical blazed transmission gratings in a coherently driven three-level atomic system using intensity-modulated images in coupling fields. Also, we analyze the feasibility of high-speed (megahertz) modulation for the induced gratings by means of image-bearing flat-top pulse trains. Consequently, continuous-wave probe fields can be efficiently and rapidly deflected in free space. When more sophisticated images are adopted, our scheme can provide further possibilities of all-optical beam splitting and fanning.

DOI: 10.1103/PhysRevA.82.013809 PACS number(s): 42.50.Gy, 42.65.An, 42.25.Fx, 42.79.−e

I. INTRODUCTION

All-optical devices play a significant role in modern optics because these devices avoid intermediate optical-electrical-optical conversion, thereby allowing high-speed performance and compact architectures. Due to its potential for all-optical control of light, electromagnetically induced transparency (EIT) is now being actively investigated [1,2]. In EIT systems, one strong coupling light field can coherently manipulate the dispersion and absorption of one weak probe light field via atomic coherence, whereby light controls light. Furthermore, when two counterpropagating coupling lasers are applied simultaneously, a standing-wave coupling field can be generated in EIT systems, which can induce various grating structures in atomic coherence. These gratings can strongly modify the propagation of probe light and thus generate stationary light pulses [3], tunable photonic stop bands [4], all-optical switching and routing devices [5], etc. On the other hand, if the standing wave is perpendicular to the propagation direction of probe light, a transverse grating, known as electromagnetically induced grating (EIG), can be generated [6,7]. EIG can diffract probe light into high-order directions, thereby splitting light beams. However, EIG produces many diffraction orders with uneven intensity and low efficiency so that it is difficult to optimally control the diffracted fields, which may limit the applications of EIG.

In some potential applications, such as free-space classical and quantum optical signal processing [8–11] and dynamic optical traps [12,13], it is important to accurately and efficiently control the directions of diffracted light fields. Here, a blazed phase grating is a powerful tool because it can diffract the incident light at a specified wavelength into one particular order [14,15]. In modern optical technologies, liquid crystal materials and microelectromechanical systems are widely used to realize tunable blazed phase gratings [16–21]. However, due to the inertia of liquid crystal molecules and mechanical components, the modulation speed of these devices is usually low (tens of kilohertz), which may cause difficulties for high-speed performance. Recently, a new proposal has shown that optical *intensity* images in coupling fields can rapidly imprint topological *phase* singularities onto probe fields in EIT systems, thus generating optical vortices [22]. The diversity of the images gives rise to various spatial structures for the modulation of probe fields, which cannot be simply produced using only standing-wave coupling fields in the EIG scheme. This advantage may provide a flexible way to enhance the functionality of EIT-based all-optical devices. Thus, if blazed phase structures can be induced for probe fields, EIT systems might be a competitive solution for all-optical redirection of light beams with high speed in free space.

In this article we theoretically study the feasibility of creating *blazed* transmission gratings in EIT systems using intensity-modulated images in coupling fields. Moreover, in order to modulate the gratings rapidly, image-bearing flat-top pulse trains could be employed, which introduce an additional frequency broadening limiting the modulation speed. We also analyze this broadening effect in detail. Consequently, we find that continuous-wave (cw) probe light beams can be efficiently and accurately deflected with high speed (megahertz) in our scheme. Based on this scheme, beam splitting and fanning are also proposed using more sophisticated images.

II. THEORETICAL MODELS AND RESULTS

In our scheme we first consider a Λ-type EIT system composed of two copropagating cw light fields interacting with a three-level atomic system in a vapor cell (Fig. 1). The weak probe light field expressed by $E_p \exp(ik_p z - i\omega_p t)$ resonantly couples the transition $|1\rangle \leftrightarrow |3\rangle$ ($\omega_p = \omega_{31}$). The strong coupling light field expressed by $E_c \exp(ik_c z - i\omega_c t)$ drives the transition $|2\rangle \leftrightarrow |3\rangle$ with a small single photon detuning $\Delta = \omega_{32} - \omega_c$. The transition dipole moments of $|1\rangle \leftrightarrow |3\rangle$ and $|2\rangle \leftrightarrow |3\rangle$ are μ_{13} and μ_{23}, respectively. The Rabi frequencies of the two light fields are denoted as $\Omega_p = \mu_{13}E_p/\hbar$ and $\Omega_c = \mu_{23}E_c/\hbar$, where $\Omega_p \ll \Omega_c$ under the EIT condition. To suppress the Doppler broadening, we also assume that the two copropagating light fields have the same frequency ($\omega_p = \omega_c$) but different polarizations and the intensity of the coupling light field is sufficiently strong. Following the derivations in Ref. [1], the steady-state solution

*zhaol@phys.tsinghua.edu.cn

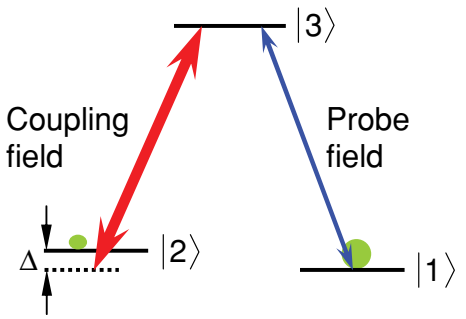

FIG. 1. (Color online) Energy-level scheme of a Λ-type atomic system driven by two copropagating light fields. Intensity-modulated images can be employed in the strong coupling field to diffract the weak probe field.

of the linear susceptibility for the cw probe field in the EIT system can be given by

$$\chi = \chi' + i\chi'' = \mu_{13}^2 N_0 \times \frac{-4\Delta\Omega_c^2 + i8\Delta^2\gamma_{31} + i2\gamma_{21d}(\Omega_c^2 + \gamma_{31}\gamma_{21d})}{\epsilon_0\hbar|\Omega_c^2 + \gamma_{31}(\gamma_{21d} - i2\Delta)|^2}, \quad (1)$$

where N_0 is the atom number density, γ_{31} is the decay rate from $|3\rangle$ to $|1\rangle$, and γ_{21d} is the decoherence rate between $|1\rangle$ and $|2\rangle$. Under the strong-coupling-field condition ($\Omega_c \gg \{\gamma_{31}, \Delta\} \gg \gamma_{21d}$), Eq. (1) reduces to

$$\chi' = \frac{-4\mu_{13}^2 N_0}{\epsilon_0\hbar}\frac{\Delta}{\Omega_c^2}, \quad (2)$$

and

$$\chi'' = \frac{2\mu_{13}^2 N_0}{\epsilon_0\hbar}\frac{4\Delta^2\gamma_{31} + \gamma_{21d}\Omega_c^2}{\Omega_c^4}. \quad (3)$$

It can be seen that when the detuning Δ is a constant and the coupling intensity is position-dependent [i.e., $\Omega_c(x,y)$], the susceptibility χ for the probe light will vary in space, which can result in the spatial phase (χ') and amplitude (χ'') modulation for the probe field.

First, we consider the spatial phase modulation. In order to generate a blazed phase grating, the coupling Rabi frequency should be chosen as a periodic form of

$$\Omega_c(x) = \frac{\gamma_{31}}{\sqrt{a\{x/w\} + b}}, \quad (4)$$

where $\{\cdots\}$ represents the fractional part of the function inside, w is the grating spacing, and γ_{31} works as a scale to evaluate the magnitude of Ω_c. The parameters a and b are x-independent constants, and their values should make $\Omega_c(x)$ satisfy the the strong-coupling-field condition mentioned earlier. According to Eq. (4), Eq. (2) can be rewritten as

$$\chi'(x) = \frac{-4\mu_{13}^2 N_0\Delta}{\epsilon_0\hbar\gamma_{31}^2}(a\{x/w\} + b), \quad (5)$$

where χ' is linear in the coordinate x and continuous in each grating period. Therefore, a *sawtooth* phase profile can be generated for the probe field in the EIT system. Here, we assume that the profile has a finite width $D = Mw$, where M is the number of periods. Additionally, the spatial intensity

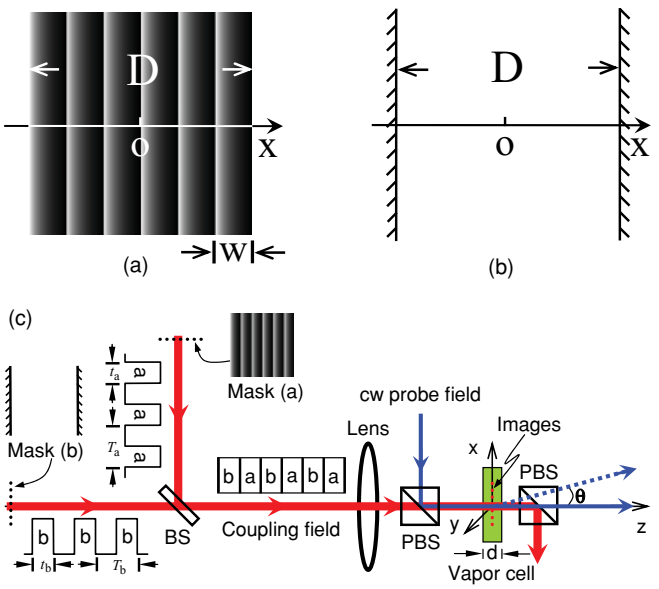

FIG. 2. (Color online) (a) Periodic intensity image in the coupling field. This image can induce a sawtooth phase profile in the EIT system to deflect the probe field. We assume that the image has a finite width $D = Mw$, where M is the number of periods and w is the spatial spacing. The intensity distribution of the image is numerically shown in Fig. 3(a). (b) Uniform coupling intensity with the same total width D and the intensity $I_{\text{uni}} = I_c(0)$, which can induce a single slit for the probe field. (c) Schematic diagram of the possible experimental setup for high-speed modulation. Two amplitude masks at the object plane of the lens can produce the corresponding images in the vapor cell at the image plane. To switch the two images rapidly, we pass two flat-top pulse trains that are complementary in the time domain through the two masks, respectively. Subsequently, the two image-bearing pulse trains are combined together behind the beam splitter. As a result, the images in the vapor cell can be switched with high speed. For simplicity, we here assume that the two pulse trains have the same repetition period $T_a = T_b = T$ and the same pulse duration $t_a = t_b = T/2$, and one pulse train is delayed for half a cycle with respect to the other. BS, beam splitter; PBS, polarizing beam splitter; θ, deflection angle.

distribution producing the x-dependent Ω_c in Eq. (4) is given by

$$I_c(x) = \frac{1}{2}\epsilon_0 c E_c^2 = \frac{\epsilon_0 c\hbar^2\Omega_c^2(x)}{2\mu_{23}^2} = \frac{\epsilon_0 c\hbar^2\gamma_{31}^2}{2\mu_{23}^2(a\{x/w\} + b)}, \quad (6)$$

where c is the speed of light in vacuum [Fig. 2(a)].

Second, we consider the spatial amplitude modulation. Using Eq. (4), Eq. (3) can be rewritten as

$$\chi''(x) = \frac{2\mu_{13}^2 N_0}{\epsilon_0\hbar}\left[\frac{4\Delta^2}{\gamma_{31}^3}(a\{x/w\} + b)^2 + \frac{\gamma_{21d}}{\gamma_{31}^2}(a\{x/w\} + b)\right], \quad (7)$$

which gives a *parabolic* absorption profile in each period accompanying the sawtooth phase profile.

The propagation of the cw probe field in the EIT system is described by Maxwell's equations. Under the paraxial

approximation (i.e., $k_{p,x} \ll k_{p,z} \approx k_p$ and $|\partial^2 E_p/\partial z^2| \ll k_p|\partial E_p/\partial z|$), the equations become

$$\frac{\partial^2 E_p}{\partial x^2} + 2ik_p\frac{\partial E_p}{\partial z} = -k_p^2 \chi E_p, \tag{8}$$

where k_p is the wave vector of the probe field. For simplicity, we only consider the beam propagation in a single slit of the induced periodic profile in the following derivations. Furthermore, within the transparency window of the EIT system, one usually has the relationship $\chi'' \ll \chi' \ll 1$. Therefore, Eq. (8) can be analogous to the Schrödinger equation describing the motion of a particle in a linear potential [23,24]. Using the quantum mechanical propagator obtained in Refs. [23,24] and considering the small χ, the probe field at the exit of the EIT system can be approximately expressed by

$$E_p^s(x,d) = \exp\left(\frac{i}{2}k_p\chi^s d\right) \times \frac{1}{\sqrt{i\lambda_p d}}\int_{-\frac{w}{2}}^{\frac{w}{2}} E_p^s(x')\exp\left[\frac{ik_p}{2d}(x-x')^2\right]dx', \tag{9}$$

where d is the thickness of the EIT vapor cell, and the superscript s denotes the quantities in the single slit. Assuming that the incident probe field is a uniform plane wave normal to the EIT system [i.e., $E_p(x') = E_p(0)$] and the Fresnel number,

$$N_F = \frac{w^2}{4\lambda_p d} \gg 1, \tag{10}$$

and then based on the derivations of the Fresnel's integrals in Refs. [14,25], we can find

$$\frac{1}{\sqrt{i\lambda_p d}}\int_{-\frac{w}{2}}^{\frac{w}{2}} \exp\left[\frac{ik_p}{2d}(x-x')^2\right]dx' \approx 1. \tag{11}$$

Therefore, under the aforementioned conditions, the transmitted probe field through the EIT system can be rewritten as the regular form,

$$E_p(x,d) = E_p(0)\exp(ik_p\chi d/2), \tag{12}$$

which also gives the transmission rate of the probe field,

$$T_p(x) = \exp[-\alpha(x)d], \tag{13}$$

where $\alpha(x) = k_p\chi''(x)$ is the absorption coefficient. Therefore, a blazed transmission grating can be induced in the EIT system, which is actually a combination of a sawtooth phase grating and an absorption grating. These two types of gratings will diffract the probe field in different manners. In addition, note that Eq. (10) gives the limit of the thickness of the EIT system, that is, $d \ll w^2/(4\lambda_p)$, which means that a thin vapor cell is preferred in our scheme.

For comparison, we also consider a uniform coupling intensity with the same total width of D and the intensity of $I_{\text{uni}} = I_c(0)$ [Fig. 2(b)]. According to Eqs. (5), (7), and (13), the uniform intensity induces the susceptibility $\chi'_{\text{uni}} = \chi'(0)$ and $\chi''_{\text{uni}} = \chi''(0)$ and the transmission rate $T_{p,\text{uni}} = T_p(0)$. Therefore, this uniform illumination actually induces a single slit in the EIT system.

Experimentally, such x-dependent spatial intensity profiles in the coupling field can be easily generated in an imaging system [Fig. 2(c)]. The amplitude masks (e.g., photographic negatives) are placed at the object plane of a lens. The thin EIT vapor cell is placed at the image plane. Consequently, the desired images in the coupling field can be reconstructed in the vapor cell.

In the following we use the ^{87}Rb D_2 line ($5\,^2S_{1/2} \leftrightarrow 5\,^2P_{3/2}$, $\lambda_p = \lambda_c = 780$ nm) as an example of the three-level atomic system to evaluate the probe light diffraction from the image-induced mixed grating. The parameters of this atomic system can be given by $\mu_{13} = \mu_{23} = 3.58 \times 10^{-29}$ C m, $\gamma_{31} = 38.11 \times 10^6$/s, $\gamma_{21\text{d}} = 2\pi \times 3000$/s, $\Delta = -0.5\gamma_{31}$, and $N_0 = 3 \times 10^{13}/\text{cm}^3$ [26]. We also assume the parameters $a = 3/2116$ and $b = 1/2116$ in Eq. (4), which can yield $23\gamma_{31} < \Omega_c(x) \leqslant 46\gamma_{31}$ to satisfy the strong-coupling-field condition. Moreover, we assume that a modulo-2π phase modulation could be imposed on the probe light field via the mixed grating, which requires

$$[\chi'(x \to w) - \chi'(x=0)]d/2 = \lambda_p \tag{14}$$

in one grating period in Eqs. (5) and (12). Therefore, one can find the thickness of the EIT vapor cell $d = 509.2$ μm. Considering the condition of Eq. (10), we assume the grating spacing $w = 200\lambda_p = 156$ μm for a large Fresnel number ($N_F = 15.3 \gg 1$). Additionally, the optical depth of the EIT system can be defined as $d_o = N_0\sigma d$, where $\sigma = 3\lambda_p^2/2\pi$ is the absorption cross section of one atom [1]. Based on the preceding parameters, the optical depth of our scheme is of the order of 4×10^3. This optical depth is a typical value in usual EIT-based slow and stored light experiments [1,2]. All the parameters are kept *fixed* throughout the rest of this article. Figure 3 numerically depicts the coupling intensity distribution, the susceptibility, and the transmission rate of our scheme based on the preceding parameters. It is worth noting that such a thin vapor cell also provides simultaneously several benefits for our scheme: (i) the image distortion in the coupling field is negligible in such a short propagation distance near the image plane, thereby allowing high-resolution images to pass through the EIT system; (ii) the absorption can be dramatically reduced [$T > 96\%$ shown in Fig. 3(c)], which means that the phase modulation for the cw probe field dominates over the amplitude modulation. In experiments, submillimeter-thin vapor cells have been fabricated [27,28]. Moreover, antirelaxation wall coatings of octadecyltrichlorosilane have been successfully prepared to suppress the collisional decoherence between the lower levels, and the Rb vapor density can be obtained up to $9 \times 10^{13}/\text{cm}^3$ [29,30]. Therefore, combining these two techniques, the thin vapor cells required in our scheme can be realized.

To calculate the far-field diffraction pattern of the probe field from the mixed grating, we first assume that the normally incident plane wave has unit amplitude [i.e., $E_p(0) = 1$]. In the Fraunhofer regime, the angular distribution of the diffraction intensity of the probe field can be expressed by [7,14,15,25]

$$I_{\text{diff}}(\theta) \propto \left|\int_{-\infty}^{+\infty} E_p(x,d)\exp(-ik_p x\sin\theta)dx\right|^2, \tag{15}$$

where θ is the diffraction angle with respect to the incident direction (the z axis). Note that $I_{\text{diff}}(\theta)$ is the *resulting* intensity distribution including the diffraction effects from both phase

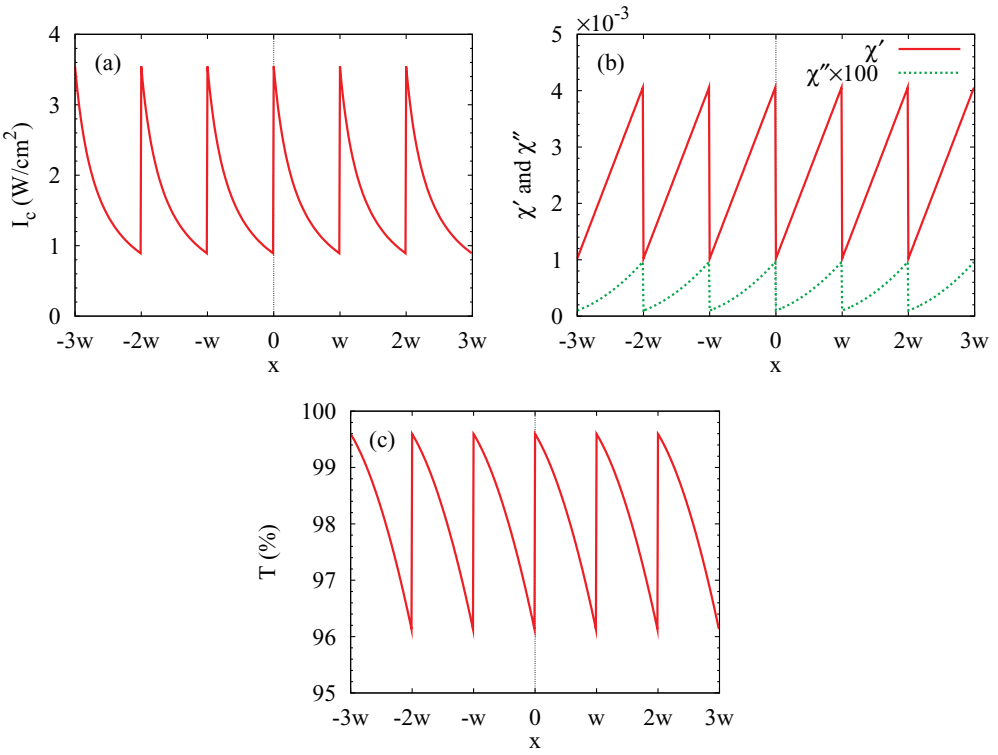

FIG. 3. (Color online) (a) Numerical illustration of the intensity distribution of the image of Fig. 2(a) in the coupling field based on Eq. (6), where $I_c(x=0)=3.54\,\mathrm{W/cm^2}$ and $I_c(x\to w)=0.89\,\mathrm{W/cm^2}$. The image has six periods (i.e., $M=6$) with the spacing $w=200\lambda_p=156\,\mu$m. (b) The induced x-dependent susceptibility χ' (solid curve) and χ'' (dotted curve). A mixed grating including both phase and amplitude modulation is generated for the probe field. (c) High transmission rate ($T>96\%$) for the probe field, which leads to a weak amplitude modulation.

and amplitude modulation. Because the entire grating contains M spatial periods, the normalized diffraction intensity can be rewritten as

$$I^{\mathrm{N}}_{\mathrm{diff}}(\theta)=\left|\frac{\sin(Mk_pw\sin\theta/2)}{M\sin(k_pw\sin\theta/2)}\right|^2\times\left|\tilde{c_1}\int_0^w E_p(x,d)\exp(-ik_px\sin\theta)dx\right|^2, \quad (16)$$

where the fractional term gives the normalized interference pattern from the multiple periods, and $\tilde{c_1}$ is the normalization coefficient for the integral term representing the diffraction from a single grating period when no absorption appears. The total width of the grating is $D=Mw$. For comparison, we also calculate the Fraunhofer diffraction pattern from the uniform coupling intensity with the same width of D [Fig. 2(b)]. In Fig. 4, it is clearly seen that the probe field can be efficiently and accurately deflected through an angle of 5 mrad due to the modulation effect of the sawtooth phase grating. The absorption grating only slightly lowers the intensity of the principal maximum. Therefore, an efficient blazed transmission grating can be generated in the EIT system to deflect the probe field.

To realize high-speed modulation in EIT systems, pulsed coupling fields can be employed in experiments [5]. Inspired by this idea, we propose a possible method as follows to implement high-speed deflection in our scheme. In this method, the coupling field should be rapidly switched between different images, such as the periodic intensity image [Fig. 2(a)] and the uniform illumination [Fig. 2(b)], and thus the directions of the diffracted beams can be changed through

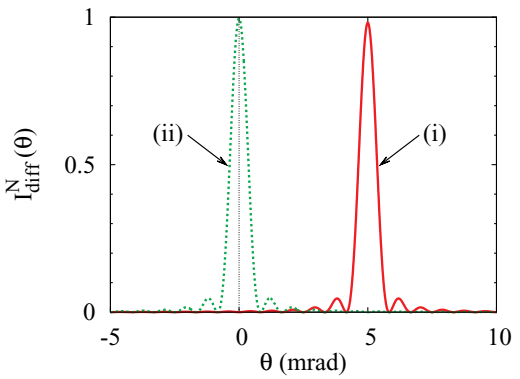

FIG. 4. (Color online) Fraunhofer diffraction patterns of the probe field from (i) the mixed grating (solid curve) with $M=6$ and $w=200\lambda_p=156\,\mu$m, and (ii) the uniform coupling intensity (dotted curve). It is clearly seen that the mixed grating can accurately and efficiently deflect the probe field into the blaze angle of 5 mrad although the principal maximum is slightly less than unity ($\sim$98%) due to the small absorption of the grating, whereas no deflection occurs for the uniform coupling intensity. Additionally, the deflection angle satisfies the grating equation [$\theta=\sin^{-1}(\lambda_p/w)$] for the $+1$st diffraction order, which confirms that the phase modulation is predominant in our scheme.

the angle of 5 mrad. Practically, image-bearing flat-top pulse trains can be used to switch the images rapidly [Fig. 2(c)]. However, the pulse trains impose a frequency broadening δf ($\approx 1/T$) on the coupling field, where T is the repetition period of one pulse train. This broadening represents the modulation speed in our scheme. To determine the speed limit, some factors should be taken into account. First, we should consider the re-establishment time of EIT [31,32]. Assuming that the initial coupling field carries the image in Fig. 2(a), then the image is switched to the uniform illumination in Fig. 2(b). The strongest absorption occurs at $x \to w$ in the first period, which gives the longest re-establishment time $\tau_r = \alpha d\gamma_{31}/\Omega_{\rm uni}^2 = 3.1$ ps, where α is the absorption coefficient given in Eq. (13) and $\Omega_{\rm uni} = \Omega_c(0) = 46\gamma_{31}$. The second factor is the time scale for validating the adiabatic approximation for the EIT system, which is given by $\tau_a = \gamma_{31}/\Omega_{\rm uni}^2 = 77.9$ ps [1,33]. Furthermore, the transparency width [$\delta f_{\rm trans} = \Omega_{\rm uni}^2/(2\pi\gamma_{31}\sqrt{d_o}) = 192.7$ MHz] and the dispersion width [$\delta f_{\rm dis} = \Omega_{\rm uni}^2/(\gamma_{31}d_o) = 18.2$ MHz] of the EIT system are two important factors as well, where d_o is the optical depth of the EIT system [1]. Thus, the modulation speed can be estimated from the limit of $\delta f \ll \{1/\tau_r, 1/\tau_a, \delta f_{\rm trans}, \delta f_{\rm dis}\}$, which means that megahertz modulation is possible in our scheme. Additionally, because the coupling intensity is not completely turned off during the fast modulation, the high transmission rate can be maintained for the cw probe field. In general, strong coupling intensity and small thickness of atomic ensembles can lead to fast response and large bandwidth of EIT systems [1,34]. Our scheme takes advantage of these two important characteristics to realize all-optical modulation with high speed. Therefore, many applications, including optical switches and routers and dynamic optical traps for ultracold atoms and molecules, could be made based on our scheme, which might be more efficient or more rapid than some existing techniques [5,12,13].

Based on the induced blazed grating structure, beam splitting and fanning can also be achieved using more sophisticated images in the coupling intensity. For beam splitting, one can design the image in the coupling intensity in the way shown in Fig. 5, which has a symmetric intensity distribution with respect to the y axis, giving domains I and II. The corresponding coupling Rabi frequency can be given by

$$\Omega_c(x) = \frac{\gamma_{31}}{\sqrt{a\{|x|/w\} + b}}. \tag{17}$$

In the right half plane (domain I), the condition for the modulo-2π phase modulation can be expressed by

$$[\chi'(x \to w) - \chi'(x = 0)]d/2 = \lambda_p \tag{18}$$

in one grating period. In the left half plane (domain II), we have

$$[\chi'(x \to -w) - \chi'(x = 0)]d/2 = \lambda_p. \tag{19}$$

Therefore, the two domains have opposite blaze directions. The intensity distribution, the susceptibility and the transmission rate of the EIT system are numerically shown in Fig. 6 using the parameters in ^{87}Rb. We can calculate the far-field angular

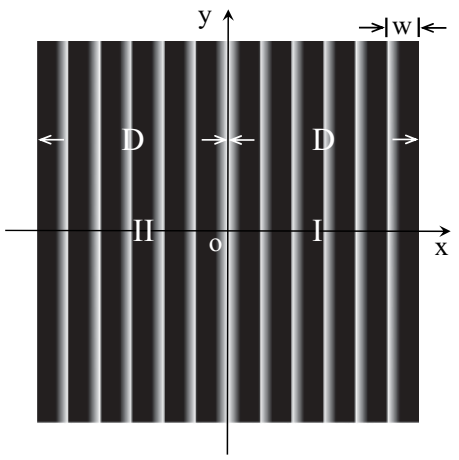

FIG. 5. Intensity image in the coupling field to split the probe field, which has two domains on both sides of the y axis. The number of periods in each domain is $M = 6$ and the spacing is $w = 200\lambda_p = 156\ \mu$m.

intensity distribution of the diffracted probe field

$$I_{\rm diff}^{\rm N}(\theta) = \left|\frac{\sin(Mk_p w\sin\theta/2)}{M\sin(k_p w\sin\theta/2)}\right|^2 \times \left|\tilde{c_2}\int_0^w E_p(x,d)\cos\{k_p\sin\theta[x + (M-1)w/2]\}dx\right|^2. \tag{20}$$

In Fig. 7, it is clearly seen that the incident probe field is split into two beams of equal intensity, and the angular separation is 10 mrad. In principle, this phase configuration is similar to a *Fresnel biprism* that can split the wave front of the incident probe field.

For beam fanning, we consider a two-dimensional (2D) image in the coupling intensity, as shown in Fig. 8(a). The corresponding Rabi frequency is given by

$$\Omega_c(x,y) = \frac{\gamma_{31}}{\sqrt{a\{[U(xy)|x| + U(-xy)|y|]/w\} + b}}, \tag{21}$$

where U is the unit step function. Therefore, one can see an array of blazed gratings with four domains in the coordinate plane. Each domain can induce an independent blazed phase structure as previously illustrated in Fig. 3. However, in the neighboring domains (e.g., domains I and II), the blazed phase gratings have orthogonal orientations. In the diagonal domains (e.g., domains I and III), the blazed phase gratings have the same orientation, but opposite blaze directions. These particular configurations may cause the incident probe field to fan out in different directions. The 2D coupling intensity distribution, the susceptibility, and the transmission rate can be obtained according to Eqs. (4)–(7). For simplicity, these quantities are not numerically shown here. We also assume that each domain has a finite area. For example, domain I is a square having the width $D = Mw$ in both x and y directions. Similar to Eqs. (16) and (20), we can perform the Fraunhofer diffraction integral in 2D and find the far-field

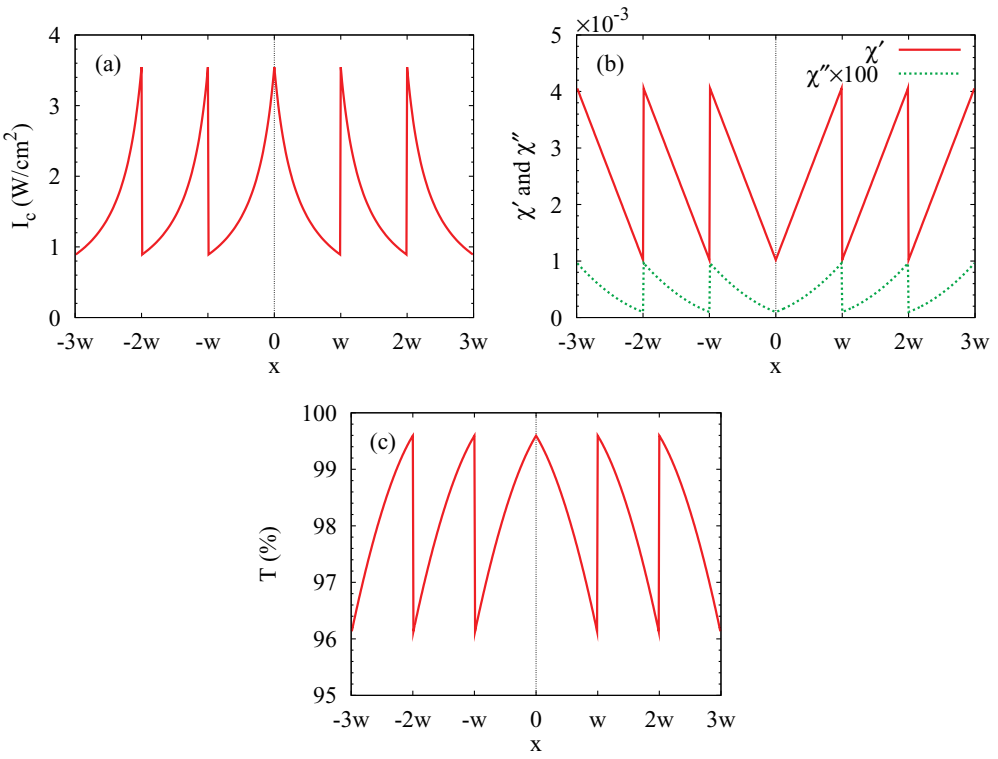

FIG. 6. (Color online) (a) Numerical illustration of the intensity distribution of the image of Fig. 5 in the coupling field, where $I_c(x=0) = 3.54$ W/cm^2 and $I_c(x \to w) = I_c(x \to -w) = 0.89$ W/cm^2. For simplicity, only three periods are shown in each domain. (b) The induced x-dependent susceptibility χ' (solid curve) and χ'' (dotted curve). A symmetric blazed grating can thus be generated to split the probe field. (c) High transmission rate ($T > 96\%$) for the probe field.

diffraction pattern [Fig. 8(b)]. Our results confirm that the incident probe field can fan out into four beams in space. The number of fan-out beams equals the domain number, which implies that more domains can generate more fan-out beams. Because the domains are independent of each other, each of the fan-out beams can be independently controlled. Additionally, based on our previous analysis about modulation speed, both beam splitting and fanning can be performed with megahertz modulation rates, whereby multichannel all-optical systems for parallel signal processing and multiple optical traps could be realized.

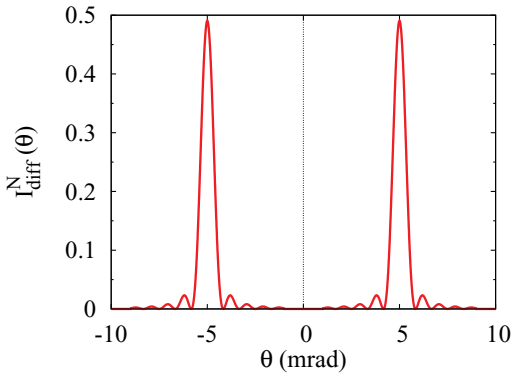

FIG. 7. (Color online) Fraunhofer diffraction pattern of the probe field from the symmetric blazed grating shown in Fig. 6. The probe field is split into two beams with the same intensity, and the separation angle is 10 mrad.

III. DISCUSSION

Finally, more discussions of our scheme should be given in the following. (i) We reconsider the Doppler effect (i.e., inhomogeneous broadening) in our scheme. Assuming that the cell temperature is 170 °C [28–30], the most probable thermal velocity of the Rb atoms is $v_p = 291$ m/s and the single-photon broadening is $\Delta\omega_D = 2\sqrt{\ln 2}k_p v_p = 3.9 \times 10^9$/s. Because the maximum deflection angle θ is 5 mrad (see Fig. 4), the two-photon Doppler broadening can be estimated by $\delta\omega_D = \theta\Delta\omega_D = 19.5 \times 10^6$/s in our scheme. Therefore, the strong-coupling-field condition (i.e., $23\gamma_{31} < \Omega_c \leqslant 46\gamma_{31}$) can yield $\Omega_c^2 \gg \Delta\omega_D\delta\omega_D$, which means that the Doppler effect can be suppressed in our scheme and Eq. (1) is a reasonable approximation for calculating the susceptibility of the cw probe field [35,36]. If one uses a light-induced atomic desorption technique, high atomic density could be obtained at relatively low temperature [37,38], which can further suppress the Doppler broadening in our scheme. While the interaction between the light fields and the nonresonant hyperfine sublevels (i.e., ac Stark shifts) may dramatically reduce the transparency of our scheme, it is possible to find level schemes to cause the compensation between these shifts and maintain the EIT effect [39]. (ii) Note that we only use the ^{87}Rb D_2 line as an example (but not the only option) to numerically evaluate our scheme. By utilizing appropriate polarization states of light fields or other atomic transitions, for example, the ladder-type configuration in Ref. [36], one could suppress some detrimental effects such as four-wave mixing

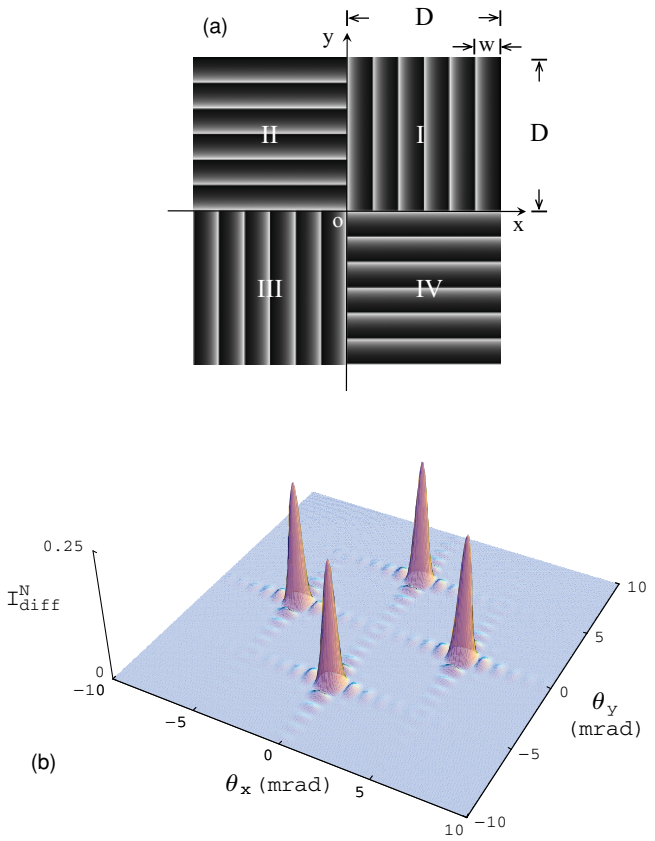

FIG. 8. (Color online) (a) Two-dimensional intensity image in the coupling field to induce the beam fanning for the probe field, where the number of grating periods in each domain is $M = 6$ and the grating spacing is $w = 200\lambda_p = 156\ \mu$m. (b) Fraunhofer diffraction pattern of the probe field. It clearly shows that the incident beam can efficiently and accurately fan out into four beams with the same intensity.

in our scheme. (iii) In Fig. 2(c), the flat-top pulse trains with megahertz repetition rates can be generated by commercial pulse generators. The pulse duration, pulse separation, rise and fall time can be precisely controlled. As long as the rise (fall) time is much shorter than the pulse duration, the overlap between the two pulse trains can be neglected, which can minimize the loss effect due to the switching between different images. In practice, the pulse trains may also come from other sources, such as the outputs of other all-optical systems. In this way, our scheme and other all-optical systems may constitute an all-optical network for signal processing. (iv) The borders between different periods would not be imaged as sharply as shown in Figs. 3 and 6 by a real lens, which blurs the borders. Severe image blur could deform the induced gratings and lower the diffraction efficiency. The blur level could be simply estimated from the lens resolution. Assuming that the diameter of the lens is $\Sigma = 5$ cm and its focal length is $f = 20$ cm, the limit of resolution with coherent illumination is given by $Y = 1.62\lambda_c f/\Sigma = 6.48\lambda_p$ [14], which is much smaller than our proposed grating period ($w = 200\lambda_p$). Also, the image quality can be enhanced even further using more advanced imaging systems [25]. Therefore, the blurred regions are only a small portion of the intensity modulated coupling images and thus have a minor influence on our scheme. (v) Notice that we use the generation of blazed phase gratings in EIT systems as an example to present the capabilities of our scheme. In fact, *other phase-modulated structures*, such as rectangular, triangular, and trapezoidal phase gratings [40], Dammann gratings [41], or the 2D sector-shaped phase structures shown in Ref. [42], could also be introduced into our scheme to realize all-optical beam splitting and fanning for the probe field.

IV. CONCLUSION

In conclusion, we have theoretically demonstrated that it is feasible to use images with periodically modulated intensity in coupling fields to create blazed transmission gratings with low absorption in EIT systems. The induced gratings can deflect cw probe fields efficiently and accurately in free space. Furthermore, we have proposed that image-bearing flat-top pulse trains can perform high-speed (megahertz) modulation for the gratings. Based on the induced blazed gratings, more sophisticated configurations can be generated using more elaborate images to enable beam splitting and fanning, where high diffraction efficiency and accuracy can be achieved with equal intensity of the diffracted beams. As a result, tunable all-optical beam deflectors, splitters and fan-out devices can be generated. These devices can efficiently and rapidly convert optical signals in the time domain (e.g., the pulse trains in coupling fields) into (multimode) optical signals in the space domain (e.g., the deflected, split and fanout probe beams). Our scheme improves the flexibility and functionality of EIT-based devices that might be useful in all-optical information processing and optical trapping and manipulation technology. Additionally, probe fields at low light levels could also be manipulated due to the low absorption in our scheme, which may have some implications for quantum information processing.

ACKNOWLEDGMENTS

This work was supported by China Postdoctoral Science Foundation, the Ministry of Science and Technology of China (Grant No. 2006CB0L0601), and the National Natural Science Foundation of China. L.Z. thanks R. Zhou and F. Peng for helpful discussions.

[1] M. Fleischhauer, A. Imamoglu, and J. P. Marangos, Rev. Mod. Phys. **77**, 633 (2005).
[2] M. D. Lukin, Rev. Mod. Phys. **75**, 457 (2003).
[3] M. Bajcsy, A. S. Zibrov, and M. D. Lukin, Nature (London) **426**, 638 (2003).
[4] M. Artoni and G. C. La Rocca, Phys. Rev. Lett. **96**, 073905 (2006).
[5] A. W. Brown and M. Xiao, Opt. Lett. **30**, 699 (2005).
[6] H. Y. Ling, Y.-Q. Li, and M. Xiao, Phys. Rev. A **57**, 1338 (1998).
[7] M. Mitsunaga and N. Imoto, Phys. Rev. A **59**, 4773 (1999).

[8] V. W. S. Chan, J. Lightwave Technol. **24**, 4750 (2006).
[9] M. Guizani and A. Battou (editors), *Optical Switching/Networking and Computing for Multimedia Systems* (Marcel Dekker, New York, 2002).
[10] C. Kurtsiefer, P. Zarda, M. Halder, H. Weinfurter, P. M. Gorman, P. R. Tapster, and J. G. Rarity, Nature (London) **419**, 450 (2002).
[11] N. Gisin, G. Ribordy, W. Tittel, and H. Zbinden, Rev. Mod. Phys. **74**, 145 (2002).
[12] V. Boyer, C. M. Chandrashekar, C. J. Foot, and Z. J. Laczik, J. Mod. Opt. **51**, 2235 (2004).
[13] V. Boyer, R. M. Godun, G. Smirne, D. Cassettari, C. M. Chandrashekar, A. B. Deb, Z. J. Laczik, and C. J. Foot, Phys. Rev. A **73**, 031402(R) (2006).
[14] M. Born and E. Wolf, *Principles of Optics*, 7th ed. (Cambridge University Press, Cambridge, UK, 1999).
[15] E. Hecht, *Optics*, 4th ed. (Addison-Wesley, Reading, MA, 2001).
[16] P. F. McManamon *et al.*, Proc. IEEE **84**, 268 (1996).
[17] X. Wang, D. Wilson, R. Muller, P. Maker, and D. Psaltis, Appl. Opt. **39**, 6545 (2000).
[18] S. Kim and L.-C. Chien, Opt. Express **12**, 1238 (2004).
[19] X. Li, C. Antoine, D. Lee, J.-S. Wang, and O. Solgaard, J. Microelectromech. Syst. **15**, 597 (2006).
[20] C. Antoine, X. Li, J.-S. Wang, and O. Solgaard, J. Lightwave Technol. **25**, 3100 (2007).
[21] M. Tormen, Y.-A. Peter, P. Niedermann, A. Hoogerwerf, H. Shea, and R. Stanley, Proc. SPIE **6114**, 61140C (2006).
[22] L. Zhao, T. Wang, and S. F. Yelin, Opt. Lett. **34**, 1930 (2009).
[23] L. S. Brown and Y. Zhang, Am. J. Phys. **62**, 806 (1994).
[24] G. P. Arrighini, N. L. Durante, and C. Guidotti, Am. J. Phys. **64**, 1036 (1996).
[25] J. W. Goodman, *Introduction to Fourier Optics*, 3rd ed. (Roberts & Co., Greenwood Village, CO, 2005).
[26] D. A. Steck, *Rubidium 87 D Line Data*, available online at [http://steck.us/alkalidata] (revision 2.1, September 1, 2008).
[27] S. Knappe, L. Hollberg, and J. Kitching, Opt. Lett. **29**, 388 (2004).
[28] A. Sargsyan, D. Sarkisyan, and A. Papoyan, Phys. Rev. A **73**, 033803 (2006).
[29] Y. W. Yi, H. G. Robinson, S. Knappe, J. E. Maclennan, C. D. Jones, C. Zhu, N. A. Clark, and J. Kitching, J. Appl. Phys. **104**, 023534 (2008).
[30] S. J. Seltzera and M. V. Romalis, J. Appl. Phys. **106**, 114905 (2009).
[31] S. E. Harris and Z.-F. Luo, Phys. Rev. A **52**, R928 (1995).
[32] H. Schmidt and R. J. Ram, Appl. Phys. Lett. **76**, 3173 (2000).
[33] M. Fleischhauer and A. S. Manka, Phys. Rev. A **54**, 794 (1996).
[34] S. E. Harris and Y. Yamamoto, Phys. Rev. Lett. **81**, 3611 (1998).
[35] M. Fleischhauer and M. O. Scully, Phys. Rev. A **49**, 1973 (1994).
[36] J. Gea-Banacloche, Y.-Q. Li, S. Z. Jin, and M. Xiao, Phys. Rev. A **51**, 576 (1995).
[37] M. Meucci, E. Mariotti, P. Bicchi, C. Marinelli, and L. Moi, Europhys. Lett. **25**, 639 (1994).
[38] A. Bogi, C. Marinelli, A. Burchianti, E. Mariotti, L. Moi, S. Gozzini, L. Marmugi, and A. Lucchesini, Opt. Lett. **34**, 2643 (2009).
[39] I. Novikova, A. B. Matsko, V. L. Velichansky, M. O. Scully, and G. R. Welch, Phys. Rev. A **63**, 063802 (2001).
[40] E. G. Loewen and E. Popov, *Diffraction Gratings and Applications* (Marcel Dekker, New York, 1997).
[41] H. Dammann and K. Görtler, Opt. Commun. **3**, 312 (1971).
[42] H. Ren and S.-T. Wu, Opt. Express **17**, 11530 (2009).